Earthquake Engineering, Tenth World Conference © 1992 Balkema, Rotterdam. ISBN 90 5410 060 5

Variation and prediction of deformation capacity of steel beam-columns

M. Nakashima
Department of Environmental Planning, Kobe University, Japan

ABSTRACT: Ductility characteristics of steel beam-columns are investigated by a survey on previous experimental data and by numerical sensitivity analysis. It was found that the ductility ratio of steel beam-columns scatters over a wide range and the material characteristics in the post yielding range are very influential to the ductility ratio. Approximate values for ensuring sufficient ductility are also presented.

1 INTRODUCTION

Ductility plays a critical role in seismic design of building structures and is given as a function of ductilities of individual structural components within the building, and therefore, it is important to quantify the ductilities of structural members. For over many decades, efforts have been made for this purpose, and numeral results, both experimental and analytical, have been accumulated. Nevertheless, in the current design specifications, provisions related to the member ductility are nothing more than vague. That is, they only state that certain conditions, like upper limits for the width-to-thickness ratio or minimum amount of reinforcement, should be satisfied to ensure a sufficient ductility, never providing us with explicit expressions for the relationship between the member ductility and other structural parameters. Seemingly, this situation is a result of wide variation in the ductility of structural members and eventual conservatism adopted in structural design. This paper reports on an effort of quantifying the degree of variation of ductility for steel beam-columns. In the first part of this paper, an extensive survey on the data obtained from previous experiments is described, and variation of ductility ratios and effects of structural parameters on them are discussed. In the second part, numerical analysis is carried out to investigate the sensitivity of the ductility ratio with respect to major structural parameters, and, in the final part, an examination is given onto how we can estimate the ductility ratio and its variation for steel beam-columns that are used in building structures.

2 SURVEY OF TEST DATA

As a means to quantify the degree of variation in the ductility ratio of steel beam-columns, an survey was conducted for previous tests. The following conditions were imposed in the survey; (1) experimental studies carried out by Japanese researchers for over the past 25 years were surveyed; (2) beam-columns having a wide flange cross section and bent in the strong axis were selected; (3) beam-columns tested in one-way (monotonic) loading were selected. As a result of the survey, a total of 224 tests out of 19 publications were chosen for the following investigation. The test data, including the geometrical and material properties, load versus deflection relationship, maximum strength, and

Table 1 Statistics of test data

Normalized Slenderness Ratio	Number of Data
$0.1 \le \bar{\lambda} < 0.2$	2
$0.2 \le \bar{\lambda} < 0.3$	75
$0.3 \le \bar{\lambda} < 0.4$	44
$0.4 \le \bar{\lambda} < 0.5$	53
$0.5 \le \bar{\lambda} < 0.6$	24
$0.6 \le \bar{\lambda} < 0.7$	18
$0.7 \le \bar{\lambda}$	8

(a) Number of data ($\bar{\lambda}$)

Axial Force Ratio (n)	Number of Data
$0.00 \le n < 0.15$	22
$0.15 \le n < 0.25$	42
$0.25 \le n < 0.35$	91
$0.35 \le n < 0.45$	39
$0.45 \le n < 0.55$	6
$0.55 \le n < 0.65$	23
$0.65 \le n$	1

(b) Number of data (n)

Type of Loading	Number of Data
DC	18
UM	26
ME	17
CL	25
TL	86
SS	52

(c) Number of data (loading condition)

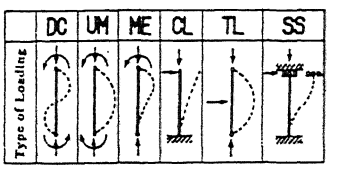

Fig.1 Type of loading condition employed in tests

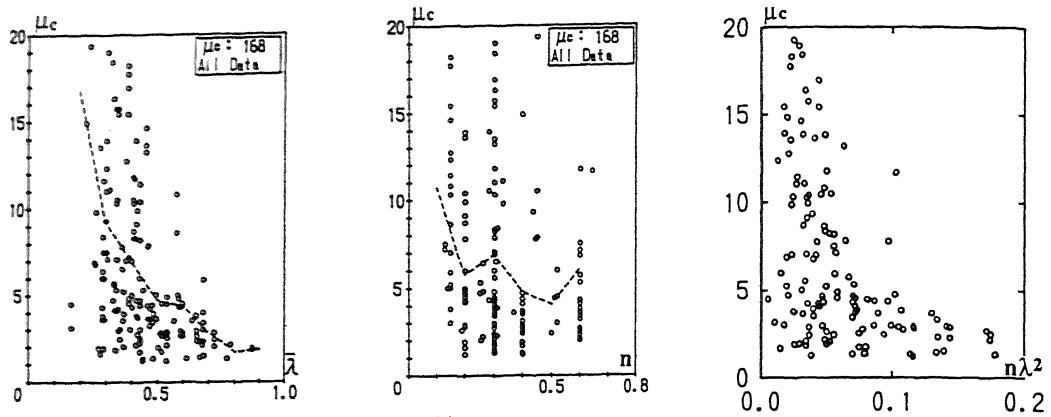

(a) with respect to $\bar{\lambda}$ (b) with respect to n (c) with respect to $n\bar{\lambda}^2$

Fig.2 Variation of experimental ductility ratios (μc)

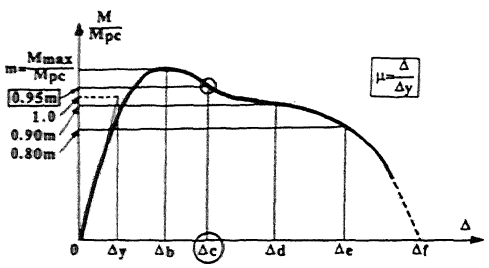

Fig.3 Definition of ductility ratios

Table 2 Means and COV of experimental ductility ratios

μc – $\bar{\lambda}$ Relationship					
$\bar{\lambda}$	Mean	COV	$\bar{\lambda}$	Mean	COV
0.15 - 0.25	16.8	0.934	0.25 - 0.35	9.3	0.655
0.35 - 0.45	7.0	0.673	0.45 - 0.55	4.7	0.741
0.55 - 0.65	4.4	0.570	0.65 - 0.75	2.8	0.394
0.75 - 0.85	1.7	0.333	0.85 - 0.95	1.8	0.032
μc – n Relationship					
n	Mean	COV	n	Mean	COV
0.05 - 0.15	10.7	0.541	0.15 - 0.25	5.8	0.606
0.25 - 0.35	6.9	0.823	0.35 - 0.45	4.8	0.876
0.45 - 0.55	4.1	0.347	0.55 - 0.65	6.1	1.351

ductility ratios, were stored in a computer in the format of a relational database. Table 1 lists the number of test data with respect to the normalized slenderness ratio ($\bar{\lambda}$), axial force ratio (n), and loading condition (shown in Fig.1). Here, the normalized slenderness ratio ($\bar{\lambda}$) was defined as the slenderness ratio about the strong axis divided by the yield slenderness ratio given by $\pi\sqrt{E/\sigma_y}$, with E and σ_y as the Young's modulus and yield stress, and the axial force ratio as the axial force imposed (which was held constant for all tests) divided by the yield axial force. For computing those quantities, the measured geometrical properties and yield stress were employed. More details in the data are given in Nakashima et al (1990, 1991). Figure 2 shows the ductility ratios (μc) with respect to $\bar{\lambda}$, n, and $n\bar{\lambda}^2$. Here, the ductility ratio (μc) is defined as the deflection corresponding to 95 % of the maximum resistance in the unstable range, divided by the yield deflection (Fig.3) Figure 2 indicates that the ductility ratios scatter over a very wide range. In fact, the ductility ratio can be 2 to 20 even for the same slenderness ratio. Table 2 lists the mean and coefficient of variation (COV) derived from Fig.2. To obtain those values, the test data were classified into small groups in accordance with either the normalized slenderness ratio or axial force ratio, and the mean and COV were estimated for each group of data. The table indicates that both the mean and COV decrease with the increase of the normalized slenderness ratio, but the magnitude of COV ranges from 0.4 to 0.9, demonstrating how large the variation of the test data was. The data were also classified by other parameters like the type of loading condition (Fig.1), width-to-thickness ratio, slenderness ratio about the weak axis, and yield ratio. It was found from respective classifications that the ductility ratio is larger in beam-columns bent in double curvature (DC, CL, TL in Fig.1) than in those bent in single curvature (UM in Fig.1), beam-columns with a smaller slenderness ratio about the weak axis is more ductile because of less strength reduction by lateral torsional buckling, and beam-columns with a larger width-to-thickness ratio is less ductile because of early local buckling. All of those observations support our common knowledge based on the first principles, but they were so only qualitatively, because the data were after all overwhelmed by large variation.

3 ANALYSIS

3.1 *Assumptions and Procedures of Analysis*

To further look into the variation of ductility of steel beam-columns, numerical analysis was carried out with various parameters that were considered to affect the ductility. The parameter chosen were (1) slenderness ratio, (2) axial force ratio, (3) type of loading condition, (4) strain hardening in the post yielding range, (5) residual stresses, and (6) initial out-of-straightness.

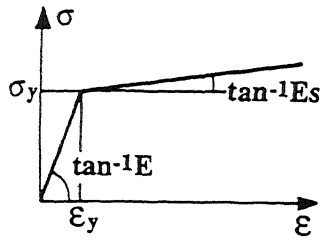

(a) Stress versus strain relationship

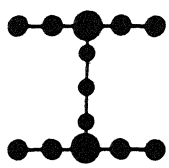

(b) Modeling of cross section

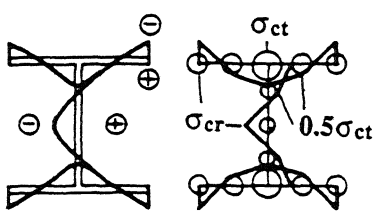

(c) Modeling of residual stresses

Fig.4 Assumptions employed in analysis

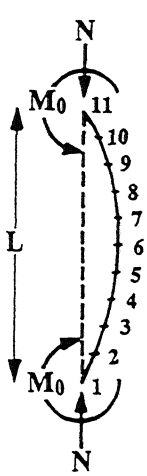

Fig.5 Modeling of beam-column

The following assumptions were employed in the analysis.

(1) The material's stress versus strain relationship was taken to be bilinear, with the initial stiffness and the stiffness in the second branch as E and Es (Fig.4(a)).

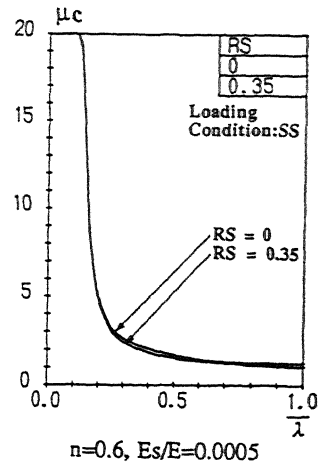

Fig.6 Effect of residual stresses on μc

In the analysis, Es/E were taken as one of 0.0005, 0.002, or 0.01.

(2) The wide-flange cross section was represented by 13 concentrated points as shown in Fig.4(b), and the moment versus curvature relationship was obtained using the assumption that the plane section remain plane after deformation.

(3) Residual stresses representative of those in hot rolled steels were considered and simplified as in Fig.4(c). In the analysis, the maximum compressive residual stress (σ_{cr}) was taken either 0 (no residual stress) or $0.35\sigma_y$.

(4) The initial out-of-straightness was given by a half sinusoidal wave. The maximum out-of-straightness, occurring in the mid-span, was taken either 0 (no out-of-straightness) or 0.002 times the beam-column's length (L).

(5) Three loading conditions: end moment at one end only (ME in Fig.1, producing the end moment ratio of 0), equal (but opposite in direction) end moments producing uniform moment distribution (UM in Fig.1), and lateral force at the top (SS in Fig.1). The other three conditions employed in the tests (Fig.1) can be approximated by the three conditions chosen in this analysis. Equal end moments producing double curvature (DC in Fig.1) can be regarded as ME with the half length, and lateral force at the top of a cantilever (CL) and lateral force at the mid-span (TL) are essentially identical with SS if their moment distributions in the plane of bending are considered.

(6) Local buckling was assumed not to occur throughout loading.

In the analysis, the length of the beam-column analyzed and its material and geometrical properties were inputted first, and then, the axial force was imposed to a magnitude specified, which was taken as one of 0.2, 0.4, or 0.6 in the axial force ratio (n). Without initial out-of-straightness, this involves no complexity, but iterative computation was required when initial out-of-straightness was present. Next, end rotation (or lateral deflection at the top in SS) was incrementally applied to the beam-column. In the computation, the beam-column analyzed was divided

into 10 segments as shown in Fig.5, and, at each boundary point, the curvature was specified in reference to the moment applied at the point. The lateral deflection (by bending) at those selected points were obtained using the moment area method and also considering the moment equilibriums at those points. Considering the parameters described above, a total of 108 combinations were given for each slenderness ratio. Analysis was carried out for normalized slenderness ratio ($\bar{\lambda}$) ranging from 0.1 to 2.0 with an interval of 0.025, and for each slenderness, a complete force versus deflection curve was obtained. The ductility ratio was obtained using the same definition as in the survey of the experimental data (Fig.3).

3.2 *Results*

Figure 6 shows an example of the ductility ratio (μc) against the normalized slenderness ratio ($\bar{\lambda}$), in which two curves, one with no residual stresses and the other with, were drawn together. As shown in this figure, the ductility ratio is hardly affected by the residual stresses; in fact, there is no difference at all for smaller slenderness ratios, where we can expect ductility. This observation appeared in all cases of analysis, and it was concluded that residual stresses are not a parameter that affect the ductility ratio significantly.

Figure 7 shows two relationships between μc and $\bar{\lambda}$, one with initial out-of-straightness and the other without, and they are the ones showing the most significant effect on the initial out-of-straightness. As shown in this figure, the difference is still marginal, and practically no difference is observed in the range where we can expect ductility. Similar to the residual stresses, the initial out-of-straightness was found not to affect the ductility ratio.

Figure 8 shows the relationships between μc and $\bar{\lambda}$, with Es/E as the parameter, demonstrating that the ductility ratio tends to increase precipitously once the normalized slenderness ratio becomes smaller than a certain ratio, and this threshold ratio is very dependent

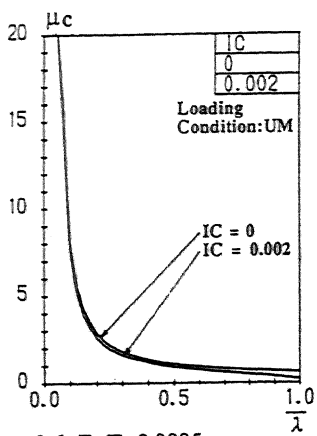

n=0.6, Es/E=0.0005

Fig.7 Effect of initial out-of-straightness on μc

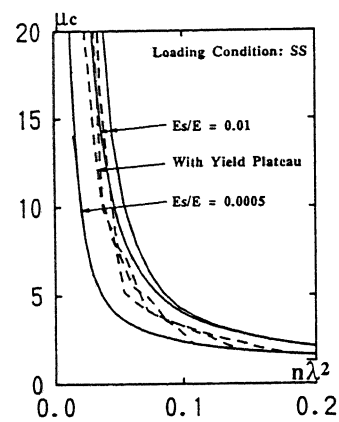

Fig.9 Effect of yield plateau on μc

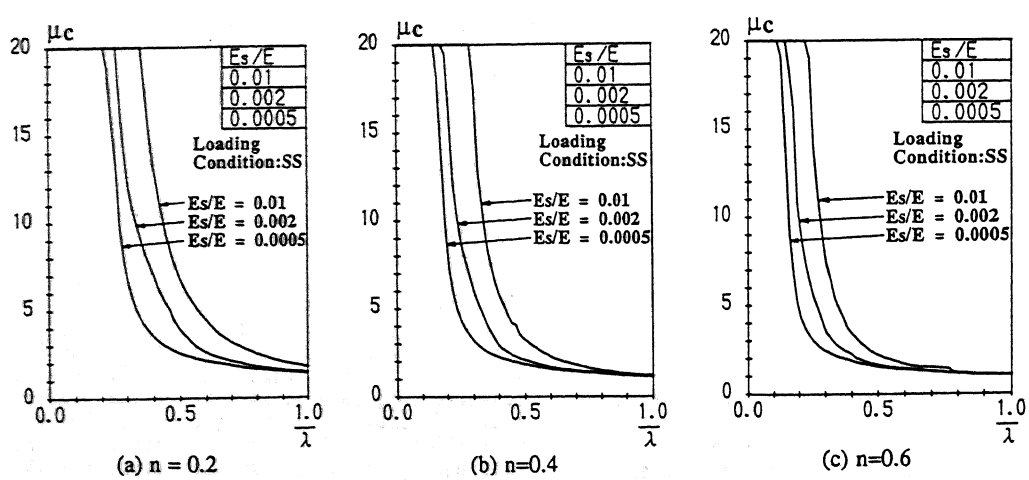

Fig.8 Effect of strain hardening on μc (no residual stresses, no initial out-of-straightness)

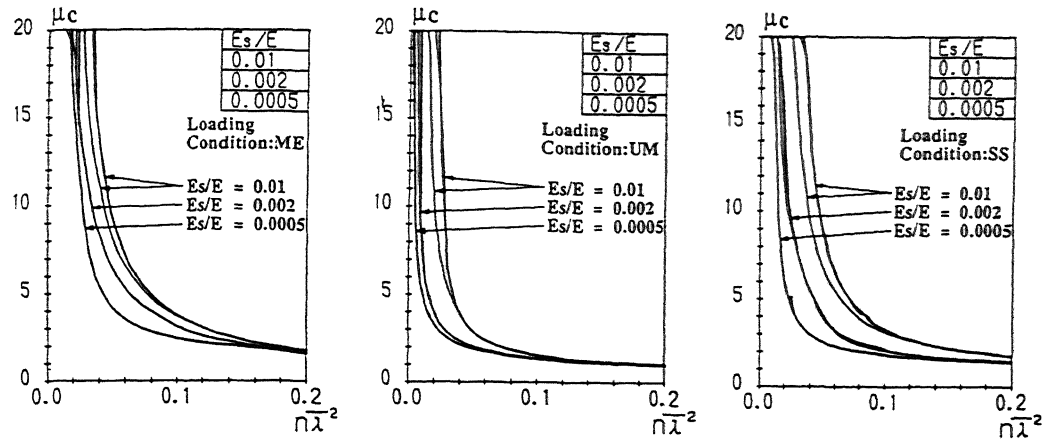

(a) Loading condition: ME (b) Loading condition: UM (c) Loading condition: SS

Fig.10 Relationship between μc and $n\bar{\lambda}^2$

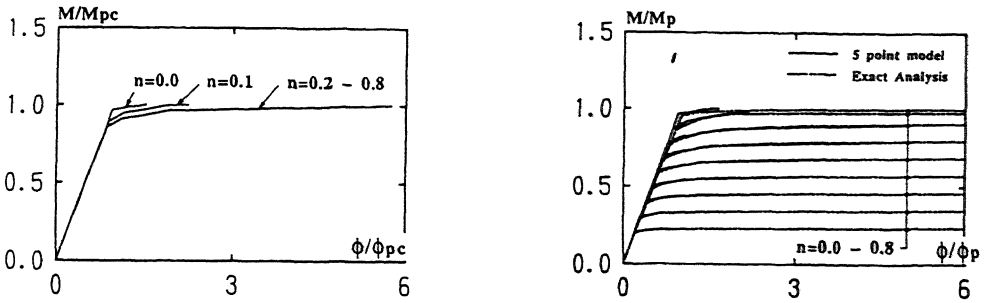

(a) Normalized moment versus curvature relationship obtained from modeled cross section

(b) Comparison in moment–curvature relationship between modeled and exact cross sections

Fig.11 Accuracy of modeled cross section

on the degree of strain hardening. In consideration of the large dependency of the ductility ratio on strain hardening, additional analysis was conducted, in which the stress versus strain relationship was assumed to be trilinear, with the initial stiffness as E, the stiffness at the second branch as 0.0005E (which represents a yield plateau), and the stiffness at the third branch as 0.01E. One of the results is illustrated by broken lines in Fig.9, which also shows the results with the bilinear relationship. This figure indicates that the yield plateau also affects the ductility ratio significantly and makes the relationship between μc and $\bar{\lambda}$ more complex. This figure reinforces the statement that the ductility ratio is influenced significantly by the material's characteristics in the post yielding range.

4 EVALUATION

In Fig.10, the relationships of Fig.8 are redrawn, but, this time, the abscissa is changed to $n\bar{\lambda}^2$. If this quantity is adopted, the three curves (with different axial force ratios) merge into one curve. Further analysis revealed that the relationship between the normalized moment (normalized by the plastic moment considering the axial force) and the normalized curvature is identical for the three axial force ratios: 0.2, 0.4, and 0.6 (as shown in Fig.11(a)), if the cross section is modelled as in Fig.4(b). In the meantime, the model was found to be sufficiently accurate as shown in Fig.11(b), in which two types of moment versus curvature relationships, one with this model and the other with more rigorous analysis, are compared. This finding, combined with the fact that the degree of moment amplification caused by the Pδ effect remains unchanged for the same $n\bar{\lambda}^2$, is the reason why the three curves matches when drawn with respect to $n\bar{\lambda}^2$. It should be emphasized that $n\bar{\lambda}^2$ is a good indicator for estimating the ductility ratio of steel beam-columns.

Figure 12 shows the analytical ductility ratios against $n\bar{\lambda}^2$, together with the experimental data. In this figure, selected were the data which had thick cross sections and small slenderness about the weak axis. It was found that the conspicuously scattered experimental data are almost enclosed by the two analytical curves, one with Es/E of 0.0005 (practically no strain hardening)

Table 3 $n\bar{\lambda}^2$ values for selected ductility ratios

Loading Condition	$n\bar{\lambda}^2$		
	μc=2	μc=5	μc=10
ME	0.144 - 0.173	0.043 - 0.075	0.026 - 0.043
UM	0.044 - 0.071	0.011 - 0.032	0.005 - 0.020
SS	0.128 - 0.210	0.037 - 0.080	0.021 - 0.047

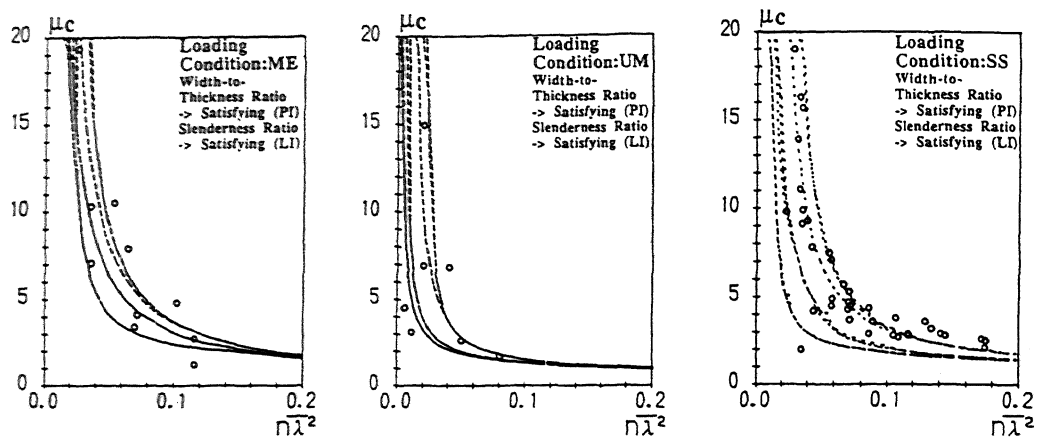

(a) Loading condition: ME (b) Loading condition: UM (c) Loading condition: SS

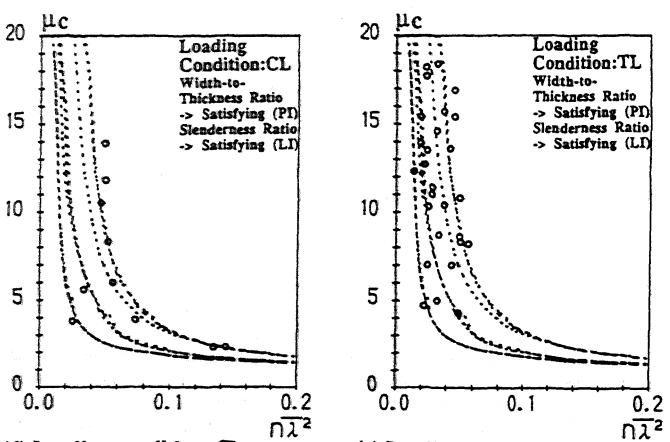

(d) Loading condition: CL (e) Loading condition: TL

Fig.12 Correlation between experimental and analytical ductility ratios

and the other with Es/E of 0.01, for all loading conditions. This observation suggests that variation caused by the difference in strain hardening is almost as large as the variation appeared in the experimental ductility ratios. Of course, we should be prudent enough so as not to hastily conclude that the material characteristics in the post yielding range are the sole source responsible for the variation of experimental data. Although the data plotted in Fig.12 are only those with thick cross sections, local buckling must be yet a factor that have affected the ductility, and one may also argue the reliability of individual test data. Despite those reservations, Fig.12 is still informative for interpreting the variation of experimental ductility ratios.

Table 3 lists the range of $n\bar{\lambda}^2$ that ensures the ductility ratios of 2, 5, and 10. These values were obtained from the results of numerical analyses, with Es/E of 0.0005 and Es/E of 0.01. The results with Es/E of 0.0005 were considered to provide us with an lower bound of the ductility ratio. In fact, a very few experimental data were below this bound. On the other hand, the results with Es/E of 0.01 were considered to give an upper bound since the curves with Es/E of 0.01 gave more or less an upper bound with respect to the experimental data. The values in Table 3 express not more than rough estimate, but such estimate is still useful to give

us a clue on specifying the range of ductile steel beam-columns.

5 CONCLUSION

The ductility characteristics of steel beam-columns were investigated by a survey on previous experimental data and also by numerical sensitivity analysis. Major findings obtained from this study are as follows:

1. The ductility ratio of steel beam-columns scatters over a wide range, with its coefficient of variation as much as 0.4 to 0.9.
2. The residual stresses and initial out-of-straightness are not the major factors that affect the ductility ratio.
3. The material characteristics in the post yielding range are very influential to the ductility ratio and can cause variation as much as that observed in the experimental data.
4. The product of the axial force ratio (n) and square of the normalized slenderness ratio ($\bar{\lambda}$) is a good indicator to estimate the ductility ratio.
5. As approximate estimate, it is suggested that $n\bar{\lambda}^2$ that ensures 5 in the ductility ratio is 0.04 to 0.08 for ME and SS and 0.01 to 0.03 for UM.

REFERENCES

Nakashima, M., S. Morino & K. Sakai 1990. Statistical evaluation of deformation capacity of steel beam-columns, *Proc. 8th Symp. Japan Earthquake Engrg.*, 2: 2055-2060.

Nakashima, M., S. Morino & S. Koba 1991. Statistical evaluation of strength of steel beam columns, *J. Struct. Engrg.*, ASCE, 117(11): 3375-3395.